



# Calculations of optical properties of the tetraphenyl-X family of isomorphous crystals (X = C, Si, Ge, Sn, Pb)<sup>†</sup>

Kacey Claborn, Bart Kahr and Werner Kaminsky\*

Department of Chemistry, Box 351700, University of Washington, Seattle, WA 98105, USA.  
E-mail: kahr@chem.washington.edu; kaminsky@wintensor.com

Received 5th March 2002, Accepted 2nd May 2002

Published on the Web 15th July 2002

Paper

As part of a program to determine how small structural changes become manifest in the optical properties of crystals we used classical dipole–dipole interaction calculations to estimate the linear birefringence and optical rotatory power of the crystals Ph<sub>4</sub>X where X = C, Si, Ge, Sn, and Pb. Field induced effects including second harmonic generation, the electro-optic response and electrogyration were calculated using the dipole electron shifting model (DES) model. The calculated induced effects are larger than those in standard materials such as KH<sub>2</sub>PO<sub>4</sub>. All of the properties tend to increase in magnitude with increasing polarizability except for optical rotation, which is largest for Ph<sub>4</sub>C. We propose an interpretation for the unusual behaviour of the optical rotation in terms of competing helical circuits of closely bonded atoms.

## Introduction

Tetraphenylmethane crystals belong to a family including the isomorphous tetraphenyl derivatives of silicon, germanium, tin and lead. This is a rare family of molecular crystals whereby a main group element in the 2nd row can be replaced by any other atom in the corresponding family, group 14 in this case, without changing the essential features of the crystal structure. As crystal engineers aspire to understand the effects of small prescribed structural changes on the physical properties of crystals, the isomorphous family, Ph<sub>4</sub>X where X = C, Si, Ge, Sn and Pb, provides unparalleled opportunities for comparison. Here, we present classical calculations of the optical properties of the Ph<sub>4</sub>X family including linear birefringence, optical rotation, as well as second harmonic generation (SHG), the electro-optic effect and induced optical rotation (electrogyration), non-linear optical effects that are of great interest to many scientists in the crystal engineering community. The parameterization of these calculations is based on redetermined experimental values of refractive indices that are at great variance with those previously reported.

## Computation methodology

### Dipole–dipole interaction

Optical rotation may be calculated using the dipole–dipole interaction theory and has been applied with success to ionic crystals.<sup>1</sup> This theory based on electronic polarizabilities is described elsewhere.<sup>2</sup> Here, we outline the basic ideas behind the calculations. Polarizability volumes were selected so that the dipole–dipole model calculations were close to the refractive indices derived experimentally.

The cumulative effect of the dipole–dipole interactions between all atoms in the crystal lattice acting on an atom *s* in unit cell *l* at a position  $r_s^l$  is described by an electrical

potential,  $V$ :<sup>2</sup>

$$V = \mathbf{Z}^l(r_s^l) = \exp(-i\omega t) \sum_s \mathbf{p}_s \exp(ikr_s^l) \times \left\{ \sum_{s'} \frac{\exp[ik_o|r_s^l - r_{s'}^l| - ik(r_s^l - r_{s'}^l)]}{4\pi\epsilon_o|r_s^l - r_{s'}^l|} \right\}$$

where  $\mathbf{Z}$  is the Hertz vector potential. The term in braces has the periodicity of the lattice. The overall Hertz potential is built from terms describing the frequency dependent incident wave, the interaction between all atoms in the unit cell and the interaction between all unit cells in the lattice, respectively.

The electric field  $\mathbf{E}(r_s^l)$  at atom  $r_s^l$  originating from the dipole waves emanating from all other atoms (point dipoles) in the structure is described by (Fig. 1):<sup>3</sup>

$$\mathbf{E}(r_s^l) = \text{grad div } V - \frac{\partial^2 V}{c^2 \partial t^2} = \sum_s A_{ss'} \mathbf{p}_{s'}^l = \alpha_s^{-1} \mathbf{p}_s^l$$

where  $\mathbf{p}_s^l$  is the electronic polarization at position  $r_s^l$  and  $\alpha_s$  is the electronic polarizability volume of atom *s*.  $A_{ss'}$  is a matrix of complex numbers.

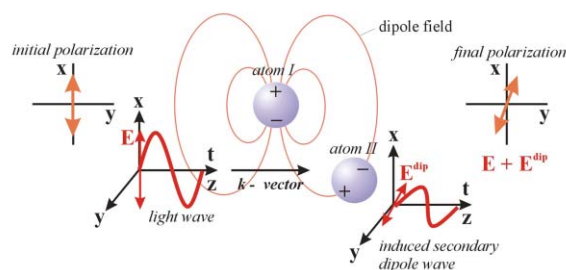


**Fig. 1** Illustration of the dipole–dipole interaction theory of Devarajan and Glazer.<sup>1</sup> When an initial wave with polarization  $\mathbf{E}$  passes the first atom positioned at  $(x,0,0)$  in a Cartesian reference system ( $z//k$ ,  $\mathbf{k}$  is the wave vector), a dipole field is created which induces in a second atom at  $(0,y,z)$  a secondary dipole field. This field oscillates in a direction different to  $\mathbf{E}$  for  $y, z \neq 0$ . The interference of all induced waves with the initial wave (calculated via an Ewald sum) on passing through the crystal leads to a rotation of  $\mathbf{E}$  when at least four atoms adopt a chiral arrangement. The result is a conversion of the atomic polarizabilities from an isotropic to an anisotropic state.

<sup>†</sup>Based on the presentation given at CrystEngComm Discussion, 29th June–1st July 2002, Bristol, UK.

Electronic supplementary information (ESI) available: virtual reality files of the representation surfaces of Fig. 4; full crystallographic data for Ph<sub>4</sub>X (X = Pb, Sn, Ge, Si, C). CCDC reference numbers 185087–185091. See <http://www.rsc.org/suppdata/ce/b2/b202304k/>

The imaginary part contained therein describes the phase shifts that result in radiative interference and optical rotation. When the sum of the contributions to the electric field is then taken the series converges only conditionally. As a remedy, the function is decomposed into a Fourier series that can be separated into two absolutely convergent parts, one in real space and the other in reciprocal space according to the Ewald theorem.<sup>4</sup>

A new matrix  $C_{ss'}$  is defined from variables describing the electric field  $\mathbf{E}(\mathbf{r}_s^i)$ :

$$C_{ss'} = (\alpha_s^{-1} \delta_{ss'} - A_{ss'} + \text{const})^{-1} = (\alpha_s^{-1} \delta_{ss'} - Q_{ss'})^{-1}$$

The imaginary part of this matrix is related to optical rotation. For the calculation of  $Q_{ss'}$  see Appendix 1. The optical rotation  $\rho(\mathbf{k})$  and optical dielectric constants  $\varepsilon_{ij}$  are derived as follows:<sup>1</sup>

$$\rho(\mathbf{k}) = \frac{-e_{rij} k_r}{2n\nu} \text{Im} \sum_{ss'} (C_{ss'})_{ij}$$

$$\varepsilon_{ij} = \delta_{ij} + \frac{1}{\nu} \sum_{ss'} (C_{ss'})_{ij}$$

( $e_{rij}$  = Levi–Civita symbol,  $\mathbf{k}$  = wave vector,  $n$  = average refractive indices,  $\nu$  = unit volume and  $\delta_{ij}$  = Kronecker delta). The Levi–Civita operation  $e_{rij}$  accomplishes the cross product between the spatial coordinates of  $C_{ss'}$  and the wave vector. The dipole–dipole interaction distorts the polarizabilities of the atoms resulting in an anisotropy described by the effective polarizabilities  $\alpha_s^{\text{eff}}$ :

$$\alpha_s^{\text{eff}} = \text{Re} \sum_{s'} C_{ss'}$$

This theoretical model reliably calculates optical rotation on the basis of the interacting forces in inorganic structures. It was further applied successfully to molecular crystals where the interacting fields within a molecule are more significant than those between the molecules.<sup>5,6</sup> Here, we are trying to evaluate the applicability of the classical theory to aromatic molecular crystals, even though we have explicitly neglected the electronic structure of the molecules in our calculations. While progress has been made in the application of quantum mechanics to the calculation of optical rotation in molecules,<sup>7</sup> in crystals we chose a theory that embodies long range interactions and accommodates the periodicity.

### Dipole electron shifting (DES)

To calculate the higher order optical properties, the classical polarizability theory was employed according to the procedure of Kaminsky and Glazer, whereby a virtual external electric field displaces the nuclei from the centers of the surrounding electron clouds in proportion to the atomic electronic polarizabilities.<sup>5</sup>

In the DES model, the external electric field shifts the atomic nuclei by distance  $\mathbf{x}$  in proportion to the polarizability of the  $k$ th atom (Fig. 2):<sup>8</sup>

$$x_i(k) = \frac{4\pi\epsilon_0}{e} \alpha_{ij}(k) E_j^{\text{loc}}$$

$e$  is the charge of an electron,  $\epsilon_0$  is the permittivity of free space and  $E_j^{\text{loc}}$  is the local electric field connected with the external field  $\mathbf{E}^{\text{ext}}$  via the effective relative dielectric constant  $\varepsilon'$  in the direction of the external field:

$$\mathbf{E}^{\text{loc}} = \frac{(\varepsilon' + 2)}{3} \mathbf{E}^{\text{ext}}$$

where a spherical depolarization field (Lorentz-depolarization) is assumed.

The largest approximation in the DES model is the substitution of the *ionic* polarizability, which should be used to

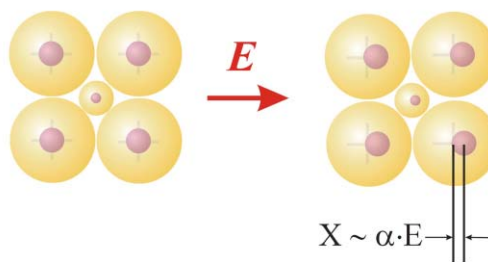


**Fig. 2** The shift of the nuclei relative to the electron clouds by an external electric field  $E$ . The radius of the clouds indicates the size of the polarizability. The external field induces a small change in the value of the electronic polarizability volumes, but this effect is neglected in the DES model. Furthermore, in the hard-spheres approximation, the electronic clouds of different atoms are not free to move relative to each other. In a classical picture at optical frequencies, the atom's nucleus is the center of the light-wave induced vibration of the shell.

calculate the shifts  $\mathbf{x}$  for static electric fields, by the *electronic* polarizability volumes. The ionic polarizabilities are not well known, in contrast to the electronic polarizabilities, which are derived from refractive indices and which are tabulated elsewhere.<sup>9</sup> Naturally, atoms with small electronic polarizabilities are only slightly affected by a static electric field.<sup>10</sup> Furthermore, if the sum of the molar polarizabilities is increased only by about a factor of three, the dielectric constant tends already to infinity, as is easily seen from the Clausius–Mosotti relation. Thus we can expect only a relatively small error by this approximation as long as the dielectric constant remains small. This is not the case when a crystal is ferroelectric, or has field dependent internal dynamics. It is of particular interest, therefore, to see if this crude approximation can be justified in the  $\text{Ph}_4\text{X}$  family.

The dipole–dipole theory was used to calculate the rotatory power  $\rho_{ij}$  ( $^\circ \text{ mm}^{-1}$ ) and the optical relative dielectric constant  $\varepsilon_{ij}$  with and without the applied field. The polarization tensor  $a_{ij}$  is the inverse of  $\varepsilon_{ij}$ :  $a_{ij} = \varepsilon_{ij}^{-1}$ ,<sup>11</sup>  $n$  is the average refractive index and  $\lambda$  is the wavelength. The dispersion of  $\alpha_{ij}$  is roughly approximated by a  $\lambda^{-1/2}$  dependence for the SHG calculations. These quantities as well as the electrogyration  $g_{ijk}$  and linear electro-optic effect at constant strain  $r_{ijk}$  were calculated from the following equations:

$$\rho_{ij}(E_k^{\text{external}}) - \rho_{ij}(0) = g_{ijk} E_k^{\text{external}} / n\lambda$$

(electrogyration at constant strain)

$$a_{ij}(E_k^{\text{external}}) - a_{ij}(0) = r_{ijk} E_k^{\text{external}}$$

(electro-optic effect at constant strain)

$$\varepsilon_{ij}(E_k^{\text{light}}) - \varepsilon_{ij}(0) = 2d_{ijk} E_k^{\text{light}}$$

(second harmonic generation).

The rotatory power  $\rho_{ij}$  is defined as the *clockwise* rotation of linear polarized light passing through a non-birefringent sample of 1 mm thickness as observed when looking towards the light source. The tensor symmetry ( $d_{ijk} = d_{ikj}$ ) was applied artificially to the calculated  $d$ -coefficients. Since  $\varepsilon_{ij} = \varepsilon_{ji}$ , the resultant  $d_{ijk}$  was totally symmetric, as expected for transparent crystals (Kleinmann's rule).<sup>12</sup> All other tensors were calculated without assuming any symmetry but nonetheless conform to Neumann's law.

## Experimental

### Crystal growth

The tetraphenyl derivatives of carbon, germanium, tin and lead were obtained from Aldrich and crystals were grown by slow

evaporation from saturated solutions of chloroform in a water bath at 30 °C. Crystals of tetraphenylsilane grown from the melt were donated by Prof. S. Haussühl (Cologne, Germany).

### X-Ray diffraction analysis

For internal consistency X-ray crystal structures of all of the members of the Ph<sub>4</sub>X family were redetermined<sup>13</sup> with a Nonius Kappa CCD diffractometer. Data were refined to  $R = 2\text{--}5\%$ . All measurements were carried out at room temperature. The hydrogen atoms on Ph<sub>4</sub>Pb were placed using a riding model. Lloyd and Brock recently presented a detailed comparative analysis of these crystal structures.<sup>14</sup> The tetraphenyl family crystallizes in the tetragonal space group  $P4_21c$  ( $D_{2d}$ ) and the molecules sit on the improper fourfold axes. In this point group there is only one independent gyration tensor element,  $g_{11} = -g_{22}$ , just as for KH<sub>2</sub>PO<sub>4</sub> and its isomorphs.

### Refractive index determination

Refractive indices were determined (Table 1) using a micron scale microscope and the three height method derived from Snell's law of refraction (Fig. 3). This 'old-fashioned' method was more reliable than the prism method because Ph<sub>4</sub>X crystals polish poorly. The birefringence measurement was refined using standard methods of polarized light microscopy confirming negative optical character throughout the series.<sup>15</sup>

The experimentally determined linear birefringence showed a strong variation that is correlated with the polarizability of the central atom.

Curiously, Newkirk reported that the refractive indices for all the crystals in the Ph<sub>4</sub>X family were essentially the same at  $1.58 \pm 0.05$ , and that the crystals were all uniaxial positive.<sup>16</sup> Both statements are incorrect. Our results are reliable within 0.01 of the absolute values and the difference between largest and smallest refractive index is 0.39.

**Table 1** Experimental refractive indices in Ph<sub>4</sub>X at 650 nm. Reliability of absolute refractive indices is *ca.*  $\pm 0.01$ .  $n_o$  and  $n_e$  are ordinary and extraordinary refractive indices perpendicular and parallel to the *c*-axis, respectively

	X = C	X = Si	X = Ge	X = Sn	X = Pb
$n_e$	1.446	1.706	1.602	1.757	1.730
$n_o$	1.476	1.742	1.647	1.840	1.789
$\Delta n$	0.030	0.036	0.045	0.083	0.050

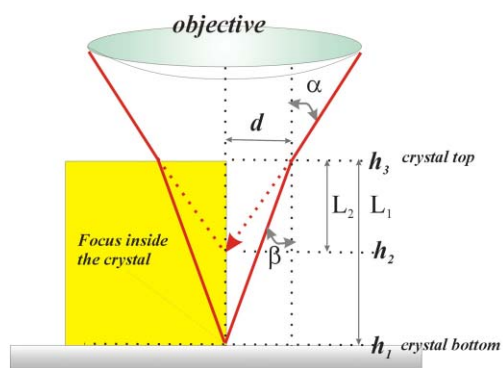


**Fig. 3** Experimental determination of absolute refractive indices using the 3-height method:

$$\frac{n}{n_{air}} = \frac{\sin\alpha}{\sin\beta} \approx \frac{\tan\alpha}{\tan\beta} = \frac{d/L_2}{d/L_1} = \frac{L_1}{L_2} = \frac{h_3 - h_1}{h_3 - h_2}$$

where  $n_{air}$  is assumed to be one.

**Table 2** Calculated optical properties at 670 nm ( $d$ -coefficients at 1064 nm) and structural details.  $\alpha_C$  (phenyl) =  $0.580 \text{ \AA}^3$ ,  $\alpha_H = 0.058 \text{ \AA}^3$ .  $\beta$ : angle between adjacent phenyl groups (see Fig. 6);  $\gamma$ : dihedral angle between phenyl rings

	X = C	X = Si	X = Ge	X = Sn	X = Pb
$\alpha_X/\text{\AA}^3$	0.62	4.50	5.00	8.80	9.50
$n_e$	1.425	1.755	1.649	1.824	1.747
$n_o$	1.455	1.667	1.608	1.833	1.767
$\rho_{11}/\text{mm}^{-1}$	252	32	-33	-75	-40
$d_{123}/10^{-12} \text{ m V}^{-1}$	-0.030	-0.094	-0.094	-2.57	-2.58
$d_{312}^2/10^{-12} \text{ m V}^{-1}$	-0.034	-0.89	-0.88	-2.47	-2.39
$\varepsilon^{-1}r_{123}/10^{-12} \text{ m V}^{-1}$	-0.273	5.8	3.5	9.2	9.2
$\varepsilon^{-1}r_{231}/10^{-12} \text{ m V}^{-1}$	1.42	7.7	4.7	11.0	9.5
$\varepsilon^{-1}g_{231}/10^{-5} \text{ V}^{-1}$	-0.14	-0.92	-0.30	-1.75	-1.87
$\beta/^\circ$	106.8	108.0	108.4	110.9	111.1
$\gamma/^\circ$	74.8	80.6	83.6	88.9	87.6
$\beta - \gamma/^\circ$	32.0	28.4	24.8	22.0	22.5
X-C/Å	1.5491	1.8730	1.9517	2.1430	2.2225
a/Å	10.9050	11.4448	11.6160	12.0680	12.1110
c/Å	7.2850	7.0640	6.9020	6.5570	6.5430

### Results of calculations and discussion

For all calculations, one needs the X-ray structure coordinates as well as the absolute refractive indices as reference. The polarizability volumes  $\alpha_H$  for hydrogen atoms and  $\alpha_C$  for carbon atoms were chosen to best match the experimental optical character. The values of  $\alpha_X$  were chosen to best match the experimental average refractive indices. In Ph<sub>4</sub>Si and Ph<sub>4</sub>Ge we could not simultaneously match the absolute values of the refractive indices and the experimental optical character. We then sacrificed the optical character, which is less important than the absolute values. The resulting estimation of optical properties is shown in Table 2 and the corresponding tensor surfaces in Fig. 4.

### Optical rotation

When employing the theory as outlined above we found a variation of the optical rotation contrary to intuition based solely on atomic polarizabilities. The calculated values of optical rotation for Ph<sub>4</sub>C, -Si, -Ge, -Sn and -Pb are 252, 32, -33, -75 and -40° mm<sup>-1</sup>, respectively (Fig. 5). Unexpectedly, the optical rotation rose sharply on going from the polarizable tin derivative to the least polarizable tetraphenylmethane.

We attempted to confirm the expectation for large optical rotations in the Ph<sub>4</sub>X family with point symmetries  $4_2m$  ( $D_{2d}$ ). Generally, however, measurements of chiro-optical properties such as optical rotation are thwarted by the much larger birefringence. We therefore had to resort to special polarimetric techniques.<sup>17</sup> In this way we confirmed that Ph<sub>4</sub>Sn was levorotatory along the absolute *a* direction determined on the basis of anomalous X-ray diffraction according to the coordinates given in Appendix 2. The error remains large because of scattering from the very soft, hard-to-polish surfaces. Small crystallites of Ph<sub>4</sub>C only extinguished with the polarizer and

optical rotation	SHG, electrooptics	electrogyration	
colors as for Ph <sub>4</sub> C	E, k parallel	E// [110]	k// [111] <sup>P</sup>

**Fig. 4** Representation surfaces in which the radius of the surface is proportional to the size of the effect. Red indicates negative signs.

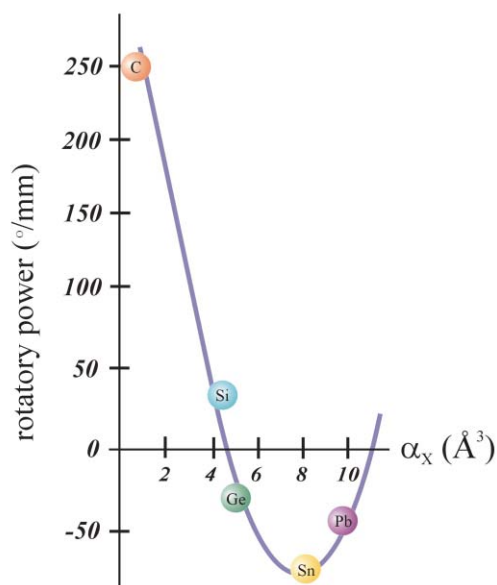


Fig. 5 Calculated optical rotation plotted against the polarizability of X in  $\text{Ph}_4\text{X}$ .

analyzer nearly parallel. This indicates a huge optical rotation in  $\text{Ph}_4\text{C}$ , which is predicted in our calculation.

For optical rotation, we venture a structural interpretation. In the propeller shaped  $\text{Ph}_4\text{X}$  molecules one can identify at least two different helical circuits of closely bonded atoms when looking toward the  $a$  axis (Fig. 6). The sense of rotation opposes the helix if the maximum of the anisotropic polarizability volumes points towards the helix axis whereas the sense of rotation follows the helix when the polarizability volumes are tangential.<sup>18</sup>

It appears that there is a competition between the two helices, 1–2–3–4–5 and A–B–C–D. The helix 1–2–3–4–5 that defines the general disposition of the phenyl rings produces dextrorotation. However, this “aromatic” optical rotation is counterbalanced by the increasing levorotation of A–B–C–D, which increases with  $\alpha_X$ . In all compounds, except  $\text{Ph}_4\text{C}$ , the polarizability volume of the phenyl carbon coordinated to the central atom (C2) was oriented radially, or towards the helix axis (Fig. 7). Thus for  $\text{Ph}_4\text{C}$ , A–B–C–D cannot counterbalance 1–2–3–4–5.

As shown in Fig. 5, the optical rotation reaches a minimum for  $\text{Ph}_4\text{Sn}$  and begins to rise again for  $\text{Ph}_4\text{Pb}$ . Nevertheless, the

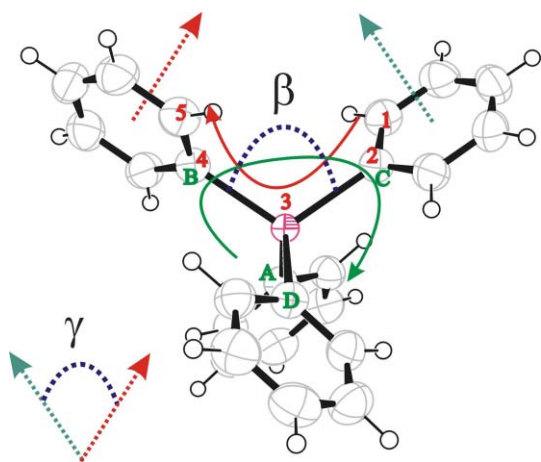


Fig. 6 Helical circuits of closely bonded atoms in  $\text{Ph}_4\text{X}$ , 1–2–3–4–5 (atoms polarized tangentially) and A–B–C–D (atoms polarized radially, except for  $\text{Ph}_4\text{C}$ ), and angles. Projection is normal to (100). Click image or here to access a 3D representation.

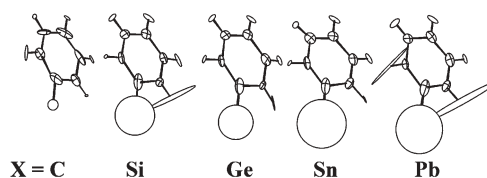


Fig. 7 Calculated anisotropic electronic polarizabilities in  $\text{Ph}_4\text{X}$ . Three hydrogen polarizabilities diverged, an unavoidable consequence of fitting the experimental refractive indices.

X–C2 bond increases throughout the series reaching a maximum length at  $\text{Ph}_4\text{Pb}$ , and thereby mitigates the opposing levorotatory influence of helix A–B–C–D. Thus, the optical rotation begins again to rise.

We also observed that the dihedral angle between phenyl groups  $\gamma$  (Fig. 6) was correlated with optical rotation. The larger the value of  $\gamma$ , the stronger the positive contribution of that helix. In fact, the torsion angle C1–C2–C4–C5 (approximated by  $\beta - \gamma$ ) followed the trend of optical rotation (Table 2, Fig. 5).

### Induced optical properties

The induced effects in each group increase by and large with increasing polarizability in accordance with the DES model, which predicts larger effects for larger polarizability differences.

It is interesting to note how the calculated electro-optic phenomena compare with commonly used materials. The values estimated for electrogyration in  $\text{Ph}_4\text{Pb}$  and  $\text{Ph}_4\text{Sn}$  reach far above the largest value reliably observed in a solid crystalline material,  $0.1 \times 10^{-5} \text{ V}^{-1}$  (normalized by the dielectric constant) in  $\text{Pb}(\text{NO}_3)_2$  along [111].<sup>19</sup> The  $d$ -coefficients are characterized by the figure of merit ( $d^2n^{-3}$ ).  $\text{Ph}_4\text{Sn}$  gives here a value of  $1.07 (\text{pm V}^{-1})^2$ . This is to be compared with  $\text{KH}_2\text{PO}_4$ ,<sup>20</sup>  $0.045 (\text{pm V}^{-1})^2$  and the best known material,  $\beta$ -barium borate,  $56 (\text{pm V}^{-1})^2$ . Newkirk cites a personal communication with Bølger and Jerphagnon concerning the  $d$ -coefficients, which are in the range of  $\text{KH}_2\text{PO}_4$ .<sup>16</sup> The calculated values for the electro-optic effect are remarkable. With expected values of the relative dielectric constants for the  $\text{Ph}_4\text{X}$  series of 5–15, the calculated electro-optic effect exceeds that in  $\text{KH}_2\text{PO}_4$  by at least a factor of 10. Newkirk also reported a large  $r_{123}$  of about  $17 \pm 1 \text{ pm V}^{-1}$  with a relative dielectric constant of about 10; neither the particular compounds measured nor the variation within the series was specified.<sup>16</sup> Yet, our calculated values were 2 to 5 times larger (Table 2).

### Alternative determination of electronic polarizability

If the estimated polarizabilities chosen to best match experimentally determined indices of refraction have realistic values, is there a way to determine them based on experiment? In general, the electronic polarizability should be in proportion to the atomic electron densities. The same is true for the X-ray scattering factors. By using the peak heights in the Fourier maps derived for structure solutions, which represent the electron densities at atoms, we hoped to find a correlation between these peak heights and the polarizabilities that were found by comparing the calculated and experimental refractive indices. The peak heights are not absolute but can be normalized to a common atom, *i.e.* the phenyl carbon atoms. The selection of electronic polarizabilities  $\alpha_X$ , fractions of peak heights, and values obtained by multiplying the fractions with the polarizability of carbon ( $\alpha_C = 0.58 \text{ \AA}^3$ ) are shown in Table 3.

For previous attempts to calculate electronic polarizabilities from X-ray structure amplitudes see Ivanov-Smolenskii *et al.*<sup>21</sup>

**Table 3** Electron density and electronic polarizability.  $P_X/P_C$  is the ratio of Fourier peak heights of atom X and the aromatic carbon, and  $\alpha_X$  is the polarizability of atom X

	X = H	X = C	X = Si	X = Ge	X = Sn	X = Pb
$P_X/P_C$	0.12	1.1	4.0	11	16	18
$\alpha_X = \alpha_C$	0.070	0.61	2.3	6.4	9.3	10
$\frac{P_X/P_C}{\alpha_X/\text{\AA}^3}$ (Table 2)	0.060	0.62	4.5	5.0	8.8	9.5

Surprisingly, we found a relatively large polarizability for aromatic hydrogen atoms derived from both estimated refractive indices and the Fourier maps.

## Acknowledgements

We are grateful to Professor S. Haussühl for donating tetraphenylsilane crystals and for financial support from the Petroleum Research Fund of the American Chemical Society (35706-AC06) and from the National Science Foundation (CHE-0092617).

## Appendix 1

$$Q_{SS'} = Q_{SS'}^0 + i \sum_{\gamma} Q_{SS'}^1 k_{\gamma}$$

$$Q_{SS'}^0 = -\frac{1}{\varepsilon_0 v R^2} \sum_{\mathbf{h}} h_{\alpha} h_{\beta} G e^{i\mathbf{h}(r_S - r_{S'})} + \frac{R^3}{4\pi\varepsilon_0} \sum_{\mathbf{l}} H_{\alpha\beta}(\mathbf{R}\mathbf{r}_{SS'}^{\mathbf{l}}) + \delta_{\alpha\beta} \delta_{SS'} \frac{R^3}{3\varepsilon_0 \pi \sqrt{\pi}}$$

$$Q_{SS'}^1 = -\frac{1}{\varepsilon_0 v R^2} \sum_{\mathbf{h}} \left[ (h_{\alpha} \delta_{\beta\gamma} + h_{\beta} \delta_{\alpha\gamma}) + \frac{2}{R^2} h_{\alpha} h_{\beta} h_{\gamma} G' e^{i\mathbf{h}(r_S - r_{S'})} \right] - \frac{R^3}{2\pi\varepsilon_0} \sum_{\mathbf{l}} H_{\alpha\beta}(\mathbf{R}\mathbf{r}_{SS'}^{\mathbf{l}}) \mathbf{r}_{SS'}^{\mathbf{l}}$$

$$G = \frac{\exp(-h^2/R^2)}{h^2/R^2}, \quad G' = \partial G / \partial k_{\gamma}$$

$$H_{\alpha\beta}(\mathbf{x}) = \frac{x_{\alpha} x_{\beta}}{x^2} \psi(|\mathbf{x}|) - \delta_{\alpha\beta} \Phi(|\mathbf{x}|)$$

$$\psi(|\mathbf{x}|) = 3\Phi(|\mathbf{x}|) + \frac{4e^{-|\mathbf{x}|^2}}{\sqrt{\pi}}, \quad \Phi(|\mathbf{x}|) = \frac{1}{|\mathbf{x}|^3} \operatorname{erfc}(|\mathbf{x}|) + \frac{4e^{-|\mathbf{x}|^2}}{\sqrt{\pi}}$$

$$\mathbf{r}_{SS'}^{\mathbf{l}} = \mathbf{r}^{\mathbf{l}} + \mathbf{r}_{S'} - \mathbf{r}_S$$

Indices  $\alpha$ ,  $\beta$  and  $\gamma$  refer to a Cartesian reference system and  $R$  is a parameter chosen so as to ensure convergence. The term corresponding to unit cell index  $\mathbf{l} = 0$  with  $S = S'$  is ignored in the summation over  $\mathbf{l}$ . In the summation over the face-normal vector  $\mathbf{h}$ , the term  $\mathbf{h} = (000)$  should be omitted.<sup>1</sup>

## Appendix 2

### Structure coordinates of Ph<sub>4</sub>Sn

Atom	$x/a$	$y/b$	$z/c$
Sn	0	0	0
C2	-0.0189(2)	0.1451(3)	0.1853(4)
C3	0.0539(3)	0.2333(3)	0.1674(5)
C4	0.0424(4)	0.3265(3)	0.2876(6)
C5	-0.0419(4)	0.3342(3)	0.4257(6)
C6	-0.1159(4)	0.2479(3)	0.4454(6)
C7	-0.1043(4)	0.1540(4)	0.3264(7)

## References

- 1 V. Devarajan and A. M. Glazer, *Acta Crystallogr., Sect. A*, 1986, **42**, 560.
- 2 G. Beurskens-Kerssen, J. Kroon, H. J. Endemann, J. van Laar and J. M. Bijvoet, in *Crystallography and Crystal Perfection*, ed. G. Ramachandran, Academic Press, London, 1963, p. 225; J. M. Bijvoet, A. F. Peerdeman and A. J. Van Bomel, *Nature*, 1951, **168**, 271; M. Born and M. Goepfert-Mayer, in *Handbuch der Physik*, 1933, **24**, 623; G. Bruhat and P. Grivet, *J. Phys. Radium*, 1935, **6**, 12; J. van Laar, H. J. Endemann and J. M. Bijvoet, *Acta Crystallogr., Sect. A*, 1968, **24**, 52; R. Reijnhart, PhD thesis, Delft, 1970.
- 3 J. D. Jackson, *Classical Electrodynamics, Second Edition*, John Wiley & Sons, New York, 1975, p. 220.
- 4 P. P. Ewald, *Ann. Phys.*, 1921, **64**, 253.
- 5 W. Kaminsky and A. M. Glazer, *Z. Kristallogr.*, 1997, **212**, 283.
- 6 W. Kaminsky and A. M. Glazer, *Phase Transitions*, 1997, **66**, 1.
- 7 R. K. Kondru, P. Wipf and D. N. Beratan, *Science*, 1998, **282**, 2247.
- 8 C. Kittel, *Introduction to Solid State Physics, Fifth Edition*, John Wiley & Sons, Inc., New York, 1976, p. 399.
- 9 J. R. Tessman, A. H. Kahn and W. Shokley, *Phys. Rev.*, 1953, **92**, 891.
- 10 N. W. Ashcroft and N. D. Mermin, *Solid State Physics*, Holt, Rinehart and Winston, London, 1976, p. 546.
- 11 L. Bohatý, *Z. Kristallogr.*, 1984, **166**, 97.
- 12 D. A. Kleinmann, *Phys. Rev.*, 1962, **128**, 133.
- 13 A. Robbins, G. A. Jeffrey, J. P. Chesick, J. Donohue, F. A. Cotton, B. A. Frenz and C. A. Murillo, *Acta Crystallogr., Sect. B*, 1975, **31**, 2395; V. Gruhnert, A. Kirfel, G. Will, F. Wallrafen and K. Recker, *Z. Kristallogr.*, 1983, **163**, 53; A. Karipides and D. A. Haller, *Acta Crystallogr., Sect. B*, 1972, **28**, 2889; P. C. Chieh and J. Trotter, *J. Chem. Soc.*, 1970, 911; V. Buseti, M. Mammi, A. Signor and A. Del Pra, *Inorg. Chim. Acta*, 1967, **1**, 424.
- 14 M. A. Lloyd and C. P. Brock, *Acta Crystallogr., Sect. B*, 1997, **53**, 780.
- 15 N. H. Hartshorne and A. Stuart, *Practical Optical Crystallography*, Edward Arnold Publishers, London, 1964, p. 230.
- 16 H. W. Newkirk, *J. Organomet. Chem.*, 1972, **44**, 269.
- 17 W. Kaminsky and A. M. Glazer, *Ferroelectrics*, 1996, **183**, 133; J. Kobayashi and Y. Uesu, *J. Appl. Crystallogr.*, 1983, **16**, 204.
- 18 A. M. Glazer and K. Stadnicka, *J. Appl. Crystallogr.*, 1986, **19**, 108.
- 19 H. J. Weber and S. Haussühl, *Z. Kristallogr.*, 1977, **146**, 3030; W. Kaminsky, A. Fahrenstich and S. Haussuehl, *Ann. Phys.*, 1992, **1**, 92.
- 20 J. Jerphagnon and S. K. Kurtz, *Phys. Rev. B*, 1970, **1**, 1749.
- 21 G. A. Ivanov-Smolenskii, V. G. Tsirelson and R. P. Ozerov, *Acta Crystallogr., Sect. A*, 1983, **39**, 411.